aerospace

MDPI

Article

Numerical Investigation of Non-Equilibrium Condensation in a Supersonic Nozzle Based on Spontaneous Nucleation

Saman Javadi Kouchaksaraei [1] and Mohammad Akrami [2,*]

[1] Faculty of Modern Technologies and Aerospace Engineering, Shahid Beheshti University, Tehran 19839 69411, Iran; s_javadikochaksaraii@sbu.ac.ir
[2] Department of Engineering, University of Exeter, Exeter EX4 4QF, UK
* Correspondence: m.akrami@exeter.ac.uk

Abstract: Non-equilibrium condensation involves intricate physics, making it crucial to thoroughly investigate the factors that influence it. Understanding these factors is essential for optimizing the system performance and minimizing the negative effects associated with non-equilibrium condensation. This study focused on examining the impact of various operational conditions in a saturated mode on non-equilibrium condensation within a supersonic nozzle. The operation conditions under investigation involved pressures of 25 kPa, 50 kPa, 75 kPa, and 100 kPa. Each saturation state was examined to assess its effect on various parameters, such as temperature, pressure, liquid mass fraction, droplet radius, nucleation rate, Mach number, and droplet count. A consistent pattern emerged across all samples. As the gas accelerated through the converging section of the nozzle, both pressure and temperature gradually decreased. However, upon reaching the throat and entering the divergent section, a phenomenon known as condensation shock occurred. This shock wave caused a sudden and significant spike in both pressure and temperature. Following the shock, both parameters resumed their downward trend along the remaining length of the nozzle. Interestingly, increasing the initial pressure of the gas led to a less intense condensation shock. Additionally, raising the saturation pressure at the nozzle inlet resulted in larger droplets and a higher concentration of liquid within the gas flow. By quadrupling the inlet saturation pressure from 25 to 100 kPa, a substantial 106.9% increase in droplet radius and a 9.65% increase in liquid mass fraction were observed at the nozzle outlet.

Keywords: non-equilibrium condensation; supersonic nozzle; saturation pressure; operation condition; droplet radius

check for updates

Citation: Kouchaksaraei, S.J.; Akrami, M. Numerical Investigation of Non-Equilibrium Condensation in a Supersonic Nozzle Based on Spontaneous Nucleation. *Aerospace* **2024**, *11*, 1032. https://doi.org/10.3390/aerospace11121032

Academic Editors: Kunyuan Zhang and Yongzhou Li

Received: 22 October 2024
Revised: 13 December 2024
Accepted: 16 December 2024
Published: 17 December 2024

Copyright: © 2024 by the authors. Licensee MDPI, Basel, Switzerland. This article is an open access article distributed under the terms and conditions of the Creative Commons Attribution (CC BY) license (https://creativecommons.org/licenses/by/4.0/).

1. Introduction

Nowadays, investigating the behavior of supersonic flow in industrial equipment is very important [1–3]. Supersonic separators have been developed specifically for the purpose of natural gas processing, primarily focusing on the removal of water vapor [4]. A key feature of these separators is the simultaneous presence of non-equilibrium condensation and shock waves in high-speed flows. The fundamental principle of supersonic separation relies on the non-equilibrium condensation of water vapor within supersonic flows [5–8]. Additionally, the presence of shock waves plays a beneficial role in transforming supersonic flows into subsonic flows, thereby recovering pressure and enhancing energy efficiency [9]. A deep understanding of non-equilibrium condensation is essential for the design and optimization of supersonic separators, enabling enhanced performance. Non-equilibrium condensation in a converging-diverging nozzle has been investigated in many studies [10,11]. These nozzles possess a simple geometry and, given appropriate boundary conditions, facilitate supersonic flow. The occurrence of two-phase flow in the nozzle results from non-equilibrium thermodynamics, which triggers phase change phenomena [12]. Dykas et al. [13] used Ansys CFX along with a custom CFD code to simulate wet steam flow. They focused on examining the impact of boundary conditions on flow behavior. Upon comparing the simulation results with laboratory data, it was determined that further studies were necessary to accurately simulate non-equilibrium condensation. Dykas et al. [14] studied moist steam flow through a Laval nozzle, with a particular focus on the impact of the shock wave on the liquid phase. They aimed to demonstrate the impact of shock waves on the difference between the numerical solution and the experimental data. The researchers linked the presence of the shock wave to the back pressure exerted on the system and noted that the interaction between liquid droplets and the SH shock waves W caused flow instability. Han et al. [15] emphasized the importance of mitigating the effects of condensation following non-equilibrium condensation by employing certain methods. They performed a study with a Stein founder nozzle to examine the effect of surface heating on the Wilson point. The authors observed that Thermal heating of the surface caused a shift in the location of the Wilson point downstream and resulted in a decrease in the liquid mass fraction. Based on their findings, they concluded that stator blades could be utilized for dehumidification purposes. Hric and Halama [16] presented three distinct models for non-equilibrium condensation, differentiating primarily in the additional terms included in the transport equations. The researchers examined these introduced models in both one-dimensional and two-dimensional forms within a converging-diverging nozzle. Sun et al. [17] highlighted the significance of non-equilibrium condensation as a concerning phenomenon in cryogenic engineering. They emphasized the need for an accurate model capable of describing non-equilibrium condensation. The researchers specifically investigated non-equilibrium condensation in nitrogen gas within a supersonic nozzle and examined the effects of modifying the droplet growth model on non-equilibrium condensation. Their findings demonstrated the selection of droplet growth models significantly affected the size of the droplet diameter. Lin et al. [18] devised a numerical approach to estimate nitrogen condensation within a nozzle. They employed a modified Gyarmathy model and a modified nucleation model to simulate non-equilibrium condensation. By comparing the outlet parameters under non-equilibrium condensation conditions with those of dry steam jets, they observed that the inclusion of non-equilibrium condensation resulted in increased pressure and temperature at the outlet. The researchers also noted that superheating the nitrogen gas at the inlet reduced the occurrence of non-equilibrium condensation.

Researchers have examined the impact of various techniques, including liquid droplet injection [19–21], salt particle injection [22–24], volumetric heating [25–27], surface heating [28,29], hot steam injection [30–32], and suction strategy [33–35] on non-equilibrium condensation. Their findings indicate that these techniques have an influence on the structure of non-equilibrium condensation. Talebi et al. [36] employed a semi-analytical model founded on the Eulerian-Lagrangian approach to explore the impact of volumetric heating in the converging sections of a nozzle. They demonstrated that the application of heating resulted in a reduction in the rate of mass flow. Furthermore, the researchers emphasized that the inlet conditions of the system had a major impact on the results of the heating process. Ma et al. [37] developed a dual-fluid stream method to examine the non-equilibrium condensation of water vapor. They computed thermodynamic characteristics within the model using an ideal equation of the state for gases. This model was used by the researchers to assess how extrinsic particles affected droplet condensation. According to their numerical results, adding external nuclei was a reasonable way to increase the size of condensed droplets. Zhang et al. [38] examined the influence of various superheated degrees of the inlet steam on a converging-diverging nozzle both experimentally and numerically. They contrasted their numerical findings with data from experiments, showing a strong agreement between the two. Their findings revealed that as the superheated degree increased, the nucleation rate decreased, resulting in fewer droplets being generated. Additionally, the liquid mass fraction and droplet radius decreased, and the nucleation zone shifted downstream in the flow.

Mehpeykar et al. [39,40] conducted simulations to analyze the non-equilibrium condensation in a converging-diverging nozzle. Their study focused on investigating the two-phase flow dynamics, condensation shock parameters, and their influence on the rate of entropy generation. Additionally, they explored the effects of volumetric heating and cooling on the system. Notably, the researchers observed that implementing the volumetric heating efficiently reduced the production of liquid within the nozzle.

Non-equilibrium condensation is a spontaneous phenomenon in supersonic vapor flows that can substantially alter flow parameters. The subsequent two-phase flow regime introduces additional complexities due to mass and heat transfer effects. This study aims to analyze the non-equilibrium condensation within a supersonic nozzle with the following objectives:

- An investigation into the influence of saturated initial conditions on non-equilibrium condensation in supersonic nozzle flows;
- An investigation of the condensation shock changes in supersonic nozzles by inlet conditions;
- The effect of increasing the temperature and pressure in the saturated state on the liquid phase and droplet radius.

2. Governing Equations

The flow of compressible moist steam inside the nozzle is modeled in this study using the Navier-Stokes equations. These equations take into account the phase of the mixture and are used to describe momentum, continuity, and energy equations. The specific equations used in this study are presented below, referenced as equations from [41]:

$$\frac{\partial \rho}{\partial t} + \frac{\partial (\rho u_j)}{\partial x_j} = 0 \tag{1}$$

$$\frac{\partial (\rho u_i)}{\partial t} + \frac{\partial (\rho u_j u_i + P\delta_{ji})}{\partial x_j} - \frac{\partial \tau_{ji}}{\partial x_j} = 0 \tag{2}$$

$$\frac{\partial (\rho E)}{\partial t} + \frac{\partial (\rho u_j H)}{\partial x_j} + \frac{\partial \left(q_j - u\tau_{ji}\right)}{\partial x_j} = 0 \tag{3}$$

The viscous stress tensor, denoted as τ_{ij}, is calculated using the method outlined in reference [42].

$$\tau_{ij} = \mu_{eff}\left(\frac{\partial u_i}{\partial x_j} + \frac{\partial u_j}{\partial x_i}\right) - \frac{2}{3}\mu_{eff}\frac{\partial u_k}{\partial x_k}\delta_{ij} \tag{4}$$

Based on previous studies, the "realizable k-epsilon" turbulence model is well-suited for predicting the flow behavior of high-Reynolds-number compressible fluids. This model consistently outperforms the standard k-epsilon model in various flow conditions, as detailed in reference [42].

$$\frac{\partial (\rho k)}{\partial t} + \frac{\partial (\rho k u_i)}{\partial x_i} = \frac{\partial}{\partial x_j}\left((\mu + \frac{\mu_t}{\sigma_k})\frac{\partial k}{\partial x_j}\right) + G_k + G_b - \rho\varepsilon - Y_M \tag{5}$$

$$\frac{\partial (\rho \varepsilon)}{\partial t} + \frac{\partial (\rho \varepsilon u_i)}{\partial x_i} = \frac{\partial}{\partial x_j}\left((\mu + \frac{\mu_t}{\sigma_\varepsilon})\frac{\partial \varepsilon}{\partial x_j}\right) + \rho C_1 S_\varepsilon - \rho C_2\frac{\varepsilon^2}{k + \sqrt{\nu\varepsilon}} + C_1\frac{\varepsilon}{k}C_3 G_b \tag{6}$$

where σ, G_k, and Y_M are the turbulent Prandtl number, the generation of turbulence kinetic energy, and the contribution of the fluctuating dilatation, respectively [43,44]. The liquid mass fraction and the droplet count can be expressed using Equations (7) and (8) in condensation [45–50].

$$\frac{\partial (\rho y)}{\partial t} + \frac{\partial \left(\rho y u_j\right)}{\partial x_j} = 4\pi\rho_l\rho n r^2\frac{dr}{dt} \tag{7}$$

$$\frac{\partial (\rho n)}{\partial t} + \frac{\partial (\rho n u_j)}{\partial x_j} = \rho J \tag{8}$$

$$r = \left(\frac{3y}{4\pi\rho_l n}\right)^{1/3} \tag{9}$$

The number of supercritical droplets is presented in Equation (10) [51,52]:

$$I = \frac{q_c}{1+\phi}\sqrt{\frac{2\sigma}{\pi}}m^{-3/2}\frac{\rho_v}{\rho_l}exp\left(\frac{-4\pi {r^*}^2\sigma}{3K_b T_v}\right) \tag{10}$$

where m represents the molecular mass, K_b is the Boltzmann constant, and q_c denotes the condensation coefficient. The temperature correction factor is represented in ϕ, which is defined by Equation (11) [53]:

$$\phi = 2\frac{(\gamma-1)}{(\gamma+1)}\frac{h_{lv}}{RT_v}\left(\frac{h_{lv}}{RT_v}-\frac{1}{2}\right) \tag{11}$$

Equations (12) and (13) are applied to calculate the droplet growth and critical radius [54,55]:

$$r^* = \frac{2\sigma}{\rho_l RT_v ln\left(\frac{p}{p_s(T_v)}\right)} \tag{12}$$

$$\frac{dr}{dt} = \frac{1}{\rho_l}\frac{\lambda_v}{(1+3.18Kn)}\frac{r-r^*}{r^2}\frac{T_s-T_v}{h_v-h_l} \tag{13}$$

The droplet temperature is determined using the Gyarmathy approximation, which has been extensively recognized by researchers [56–60].

$$T_l = T_s(P) - (T_s(P)-T_v)\frac{r^*}{r} \tag{14}$$

3. Numerical Method

To analyze the steady-state two-dimensional flow equations, the Reynolds-Averaged Navier-Stokes (RANS) approach was implemented, coupled with the k-ε realizable turbulence model [20,58]. A control volume method was utilized, and a density-based solver was selected to solve the governing equations. All numerical simulations were conducted using Ansys Fluent 18. Convergence was achieved when the residuals for all parameters were reduced below 10^{-6}. To accurately simulate the liquid phase behavior within Ansys Fluent, user-defined functions were necessary. However, developing a user-defined functions for non-equilibrium condensation proved to be a complex task due to the numerous interdependent parameters involved. This complexity significantly increased the challenge of integrating such a model into the software.

3.1. Geometry and Boundary Condition

The Moore B nozzle, a well-known design, has specific dimensions given in Table 1 [57]. To simulate flow, we set initial conditions at the inlet: stagnation pressure, stagnation temperature, droplet count, and liquid mass fraction. As the flow becomes supersonic at the exit, parameter values are extrapolated from the domain's interior, and pressure outlet is selected for exit. The nozzle walls are assumed adiabatic and non-slip, and the flow is symmetric about the centerline. The working fluid in this study is water vapor.

Table 1. Geometry of Moore B nozzle [57].

X [mm]	Y [mm]
−200	56.35
0	50
500	72

3.2. Mesh Study in Moore B Nozzle

Ensuring the grid independence of the numerical solution is a critical aspect in computational simulations. Examining how the number of computational cells affects the numerical solution's results is the main goal of this conversation. In this study, the pressure profile along the nozzle's centerline is utilized to assess the grid independence of the solution. The solution's independence from the grid is shown in Figure 1. Where three different numbers of cells, namely 4000, 7000, and 16,000, are employed for this investigation.

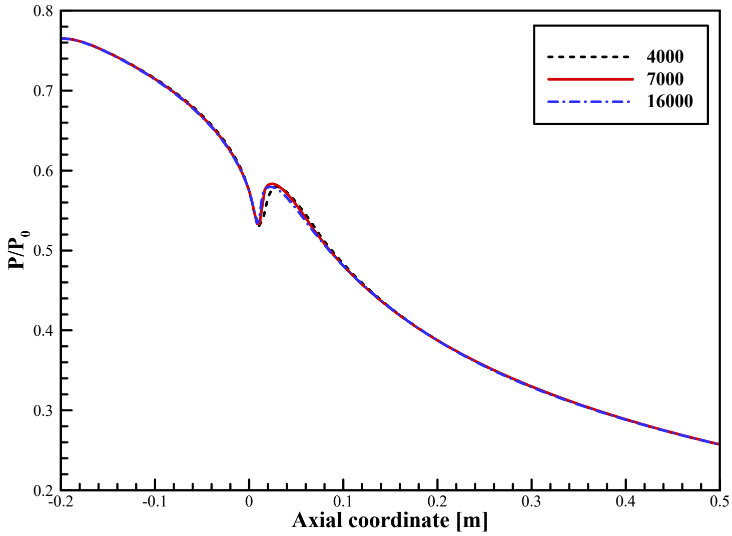

Figure 1. The effects of cell number on pressure distribution in the supersonic nozzle.

The results indicate that there is minimal difference between the solutions obtained with 7000 and 16,000 cells. Consequently, to minimize computational expenses, the number of cells chosen for this study is 7000. The optimal computational grid can be observed in Figure 2. The accuracy of the mesh simulations hinges on the y+ parameter, a dimensionless measure of distance from the wall, scaled to the boundary layer thickness [61]. Typically, the k-epsilon Realizable model works best when the y+ value falls between 30 and 300. This range maintains the accuracy of the wall functions while keeping computational costs manageable.

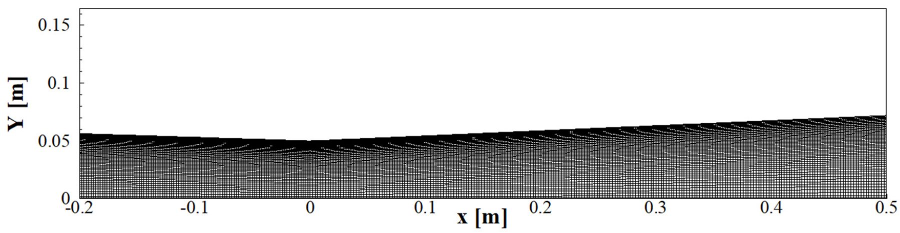

Figure 2. Computational mesh in supersonic nozzle.

3.3. Validation of Moore B Nozzle

This section focuses on validating the numerical solution with experimental data gathered from the Moore B nozzle [58]. The inlet temperature and pressure are recorded as 357.6 K and 25 kPa, respectively. The verification of the numerical solution is depicted in Figure 3. Upon examining Figure 3, it is evident that the numerical solution accurately predicts the laboratory data, indicating a good agreement between the two.

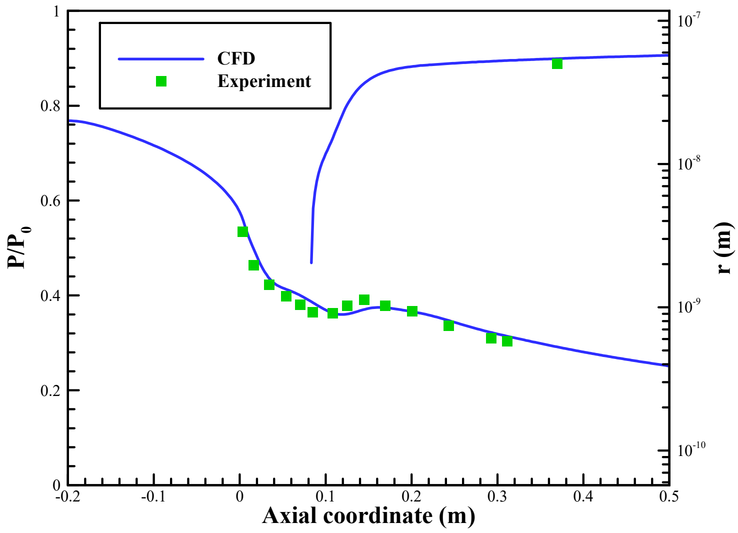

Figure 3. Validation of numerical method in supersonic nozzle.

4. Results and Discussion

The operational conditions are known to significantly influence non-equilibrium condensation. Assessing non-equilibrium condensation under saturated inlet circumstances is the primary goal of this investigation. The study considers four different saturation states for the inlet and examines the impact of each state on non-equilibrium condensation. The aim is to gain a new understanding of this phenomenon. Table 2 presents the modes that have been considered, with inlet pressures of 25 kPa, 50 kPa, 75 kPa, and 100 kPa for each mode. This section focuses on investigating the effects of each saturation state on temperature, pressure, Mach number, droplet number, nucleation rate, droplet radius, and liquid mass fraction.

Table 2. Operation condition in supersonic nozzle.

	Case 1	Case 2	Case 3	Case 4
P [kPa]	25	50	75	100
T [K]	338.1	354.5	364.9	372.9

4.1. *Effects of Operation Conditions on Pressure, Temperature and Mach Number*

Supersonic nozzles find various applications in industries, and understanding the variations in key flow parameters within these nozzles is crucial for their optimal design. The primary flow parameters of interest include temperature, pressure, and Mach number. In an ultrasonic nozzle, the temperature and pressure undergo a downward trend, implying a decrease along the nozzle. On the other hand, The Mach number exhibits an increasing trend. However, non-equilibrium condensation disrupts the flow structure and leads to abrupt changes in the main flow parameters. This abrupt change is referred to as condensation shock.

Figure 4 shows how various saturation conditions effect on the pressure profile inside the nozzle at the nozzles input. The flow inlet pressure values considered are 25 kPa, 50 kPa, 75 kPa, and 100 kPa. It is observed that the pressure change process is similar for each sample. In the convergent part of the nozzle ($x < 0$), there is a gradual decrease in pressure. Condensation shock results in an abrupt shift in pressure between the throat area and the divergent part of the nozzle. Subsequently, the pressure continues to decrease after the condensation shock. The pressure values at the nozzle outlet for each sample are 6.43 kPa, 12.71 kPa, 18.89 kPa, and 25.01 kPa, corresponding to the respective saturation states.

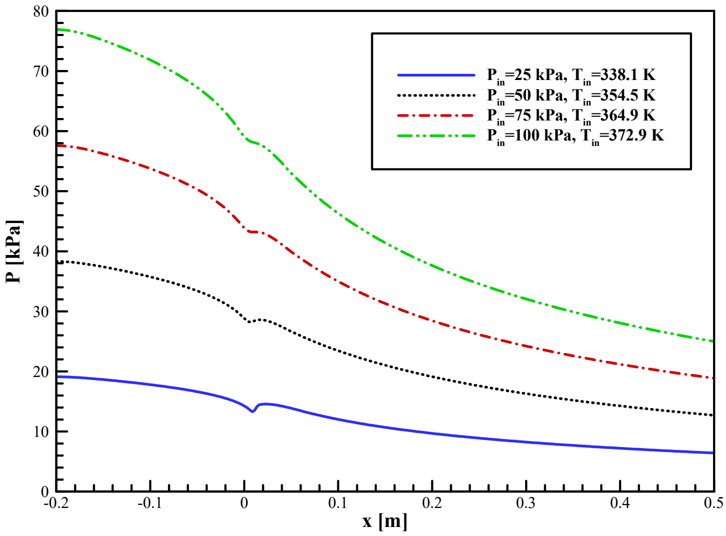

Figure 4. The effects of saturation operation conditions on pressure distribution in the supersonic nozzle.

Figure 5 illustrates the effect of different saturation conditions on the temperature distribution within the supersonic nozzle. The temperature change process is similar for each saturation state under consideration. As the saturation temperature and saturation pressure increase at the nozzle inlet, the occurrence of condensation shock takes place at higher temperatures. Specifically, for each sample, the condensation shock is observed to transpire at temperatures of 290 K, 309 K, 320 K, and 328 K, respectively.

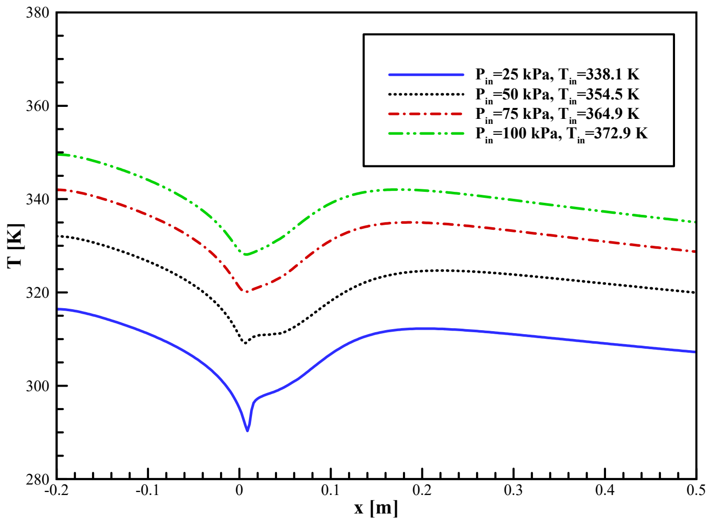

Figure 5. The effects of saturation operation conditions on temperature distribution in the supersonic nozzle.

For input pressures of 25, 50, 75, and 100 kPa, the Mach value distribution in the supersonic nozzle is displayed in Figure 6. The location of the condensation shock is also highlighted in Figure 6. Upon examining the figure, it is evident that there is minimal variation in the Mach number within the converging part of the nozzle. Nonetheless, notable alterations are seen in the divergent portion within the nozzle and the placement of the condensation shock. An increase in the intake saturation pressure causes the Mach number in the diverging part to rise. For input pressures of 25, 50, 75, and 100 kPa, the nozzle outlet's Mach number is 1.447, 1.456, 1.465, and 1.471, respectively. Furthermore, the intensity of the condensation shock is higher for the pressure of 25 compared to the other samples. As the input pressure rises, the condensation shock's strength seems to diminish, resulting in a fall in the condensation shock's Speed number.

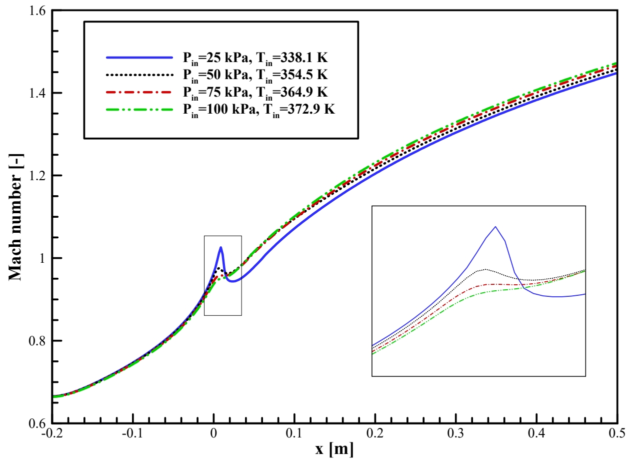

Figure 6. The effects of saturation operation conditions on Mach number distribution in the supersonic nozzle.

4.2. The Effect of Saturated Operation Conditions on Nucleation Rate, Liquid Mass Fraction, Droplet Number and Droplet Radius in Moore B Nozzle

Condensation shock significantly influences the flow pattern within the nozzle. In the preceding section, we examined the impact of saturation conditions on condensation shock and the resulting changes in flow parameters. Condensation shock occurs as a result of latent heat release during phase change. In this section, we will explore the effect of saturated operating conditions on non-equilibrium condensation parameters.

The impact of various saturation pressures on the nucleation rate in the Moore B nozzle is depicted in Figure 7. The nucleation rate is a crucial parameter in non-equilibrium condensation, representing the rate at which very fine droplets with a critical size are formed. Non-equilibrium condensation in the nozzle initiates with nucleation. It is observed that the nucleation rate decreases as the saturation pressure at the nozzle inlet increases. The highest nucleation rate is associated with a saturation pressure of 25, with a value of approximately $10^{19.65}$ 1/kg.s. Furthermore, it appears that as the saturation pressure increases, nucleation within the nozzle commences earlier.

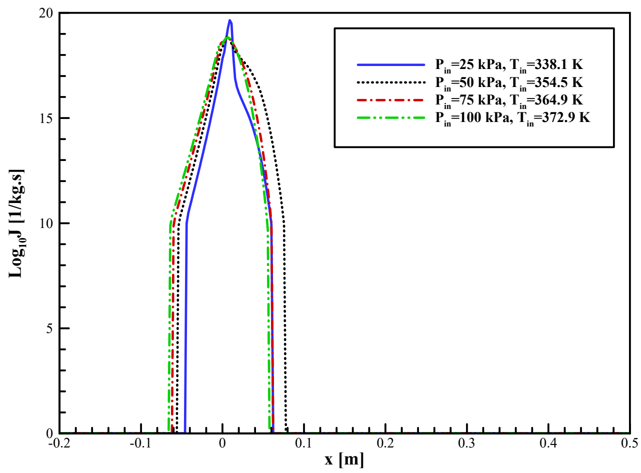

Figure 7. The effects of saturation operation conditions on nucleation rate in the supersonic nozzle.

Figure 8 displays the effect of different saturation pressures on the droplet count. The droplets formed from nucleation begin to grow, leading to an increase in their size. Increasing the saturation pressure at the nozzle inlet appears to decrease the droplet count within the nozzle. The number of liquid drops at the nozzle outlet for each saturation state is recorded as $10^{15.75}$ 1/kg, $10^{15.05}$ 1/kg, $10^{14.95}$ 1/kg and $10^{14.85}$ 1/kg, respectively. The significance of the droplet count lies in providing the necessary surface area for vapor condensation and subsequent vapor-to-liquid conversion.

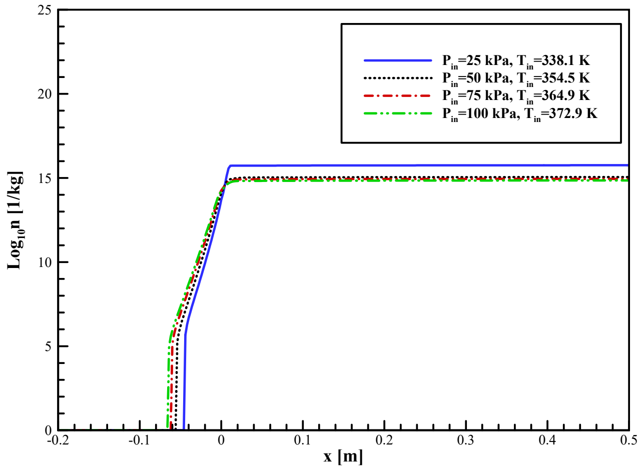

Figure 8. The effects of saturation operation conditions on droplet number in the supersonic nozzle.

Figure 9 illustrates the effect of different saturation pressures at the nozzle inlet on the droplet radius, while Figure 10 displays the changes in liquid mass fraction. Figure 9 shows that the droplet radius increased as the saturation pressure at the nozzle inlet rises. The droplet radius at the nozzle outlet for saturation pressures of 25, 50, 75, and 100 kPa was measured as 138.6 nm, 240.4 nm, 264.6 nm, and 287.0 nm, respectively. By increasing the inlet saturation pressure from 25 to 100, the droplet radius at the outlet showed an approximate 106.9% increase. This suggested a significant impact of the inlet pressure on the droplet radius.

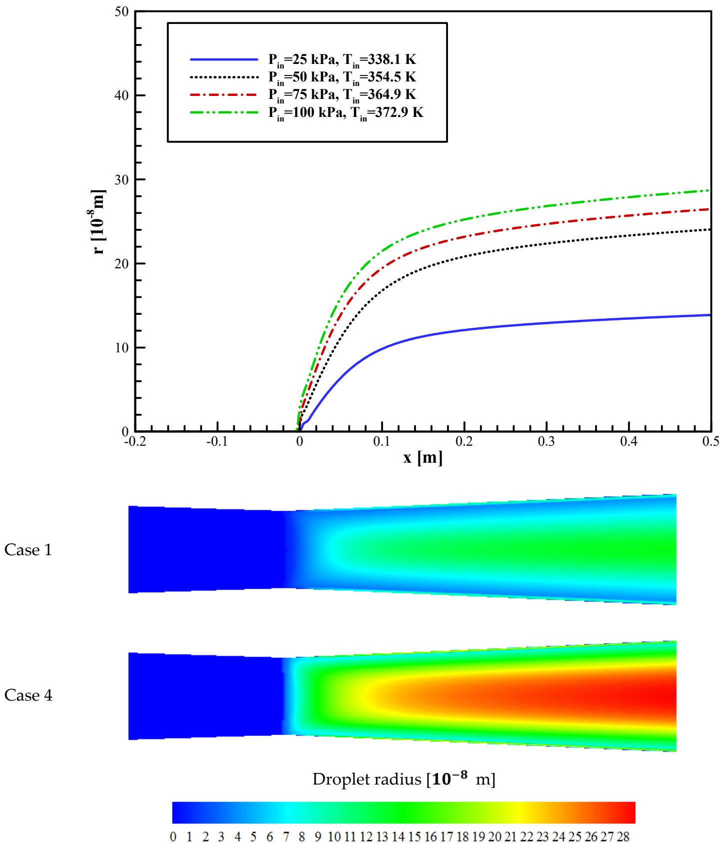

Figure 9. The effects of saturation operation conditions on droplet radius in the supersonic nozzle.

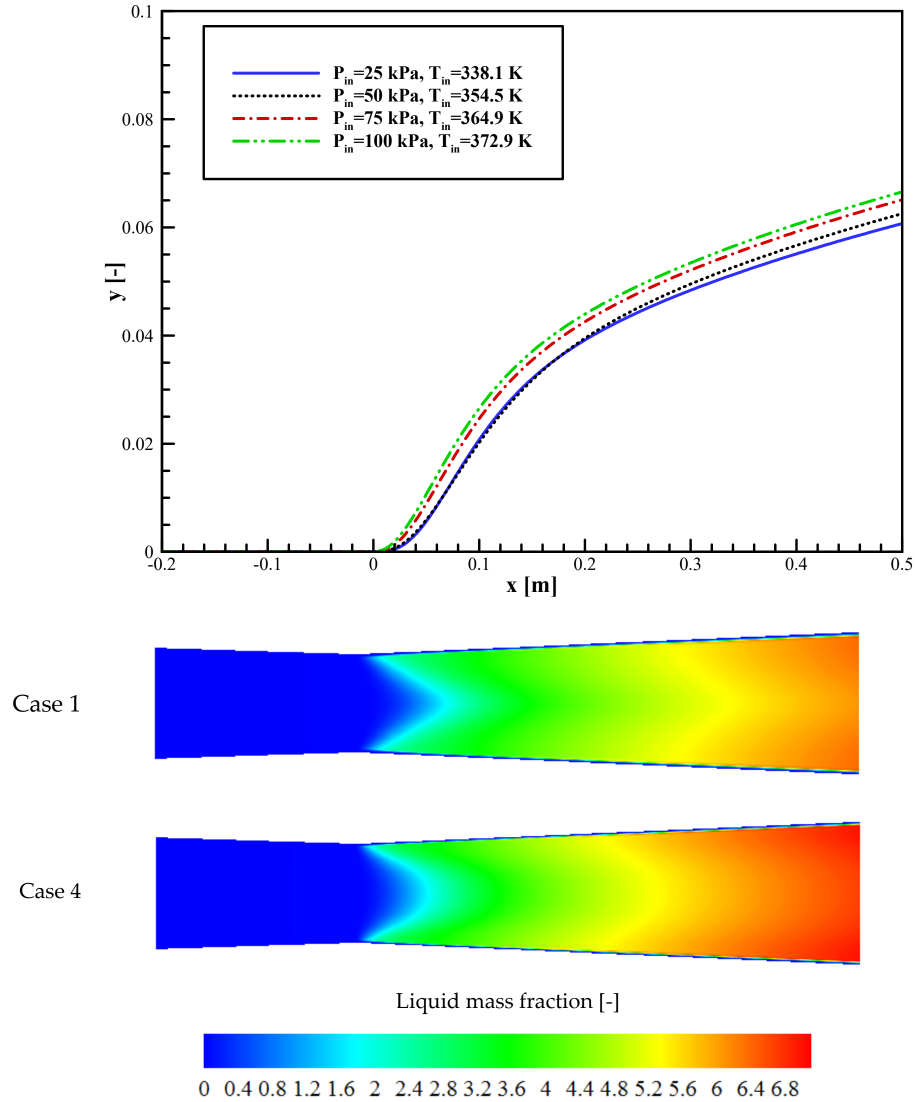

Figure 10. The effects of saturation operation conditions on liquid mass fraction in the supersonic nozzle.

Figure 10 illustrates the impact of varying inlet saturation pressure on the liquid mass fraction at the nozzle outlet. As the saturation pressure increased from 25 kPa to 100 kPa, the liquid mass fraction gradually rose, reaching values of approximately 0.0606, 0.062, 0.065, and 0.066, respectively. This translated to a modest overall increase of about 9.65% in the liquid mass fraction. However, when compared to the significant influence of saturation pressure on the droplet radius, the effect on the liquid mass fraction was relatively minor. This suggests that while increasing the saturation pressure can slightly enhance the liquid mass fraction, its primary impact lies in modifying the droplet size distribution.

4.3. The Effect of Saturated Operation Conditions on Mass Flow Rate in the Moore B Nozzle

The impact of different saturation pressures at the nozzle inlet on the flow rate is depicted in Figure 11. Increasing the inlet saturation pressure resulted in a rise in the mass flow rate inside the nozzle. Specifically, as the inlet pressure increased from 25 kPa to 100 kPa, the flow mass flow rate experienced a significant increase of approximately 281%. It was observed that an increase in the saturation pressure at the nozzle inlet resulted in a simultaneous rise in both the liquid mass fraction and the mass flow rate. This indicated that the production of the liquid phase within the nozzle was enhanced with an increase in the saturation pressure at the inlet.

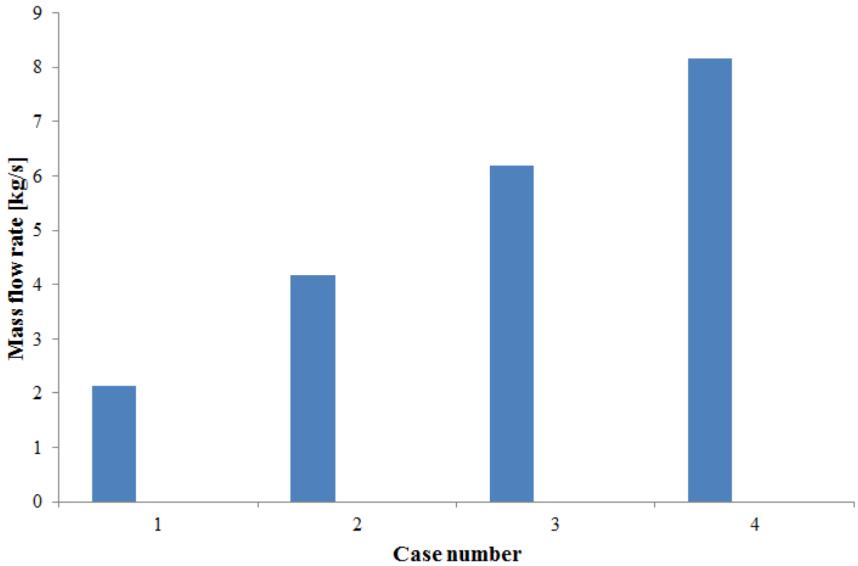

Figure 11. The effects of saturation operation conditions on mass flow rate in the supersonic nozzle.

5. Conclusions

The primary goal of this study was to explore non-equilibrium condensation under saturated inlet conditions. Four different saturation states were examined, with a focus on analyzing how each state influenced the occurrence of non-equilibrium condensation. Its primary goal was to evaluate how these distinct saturation states affected temperature, pressure, Mach number, droplet count, nucleus formation rate, drops radius, and liquid mass fraction. The following are the important conclusions drawn from this study:

- The changes observed in each of the samples displayed a consistent pattern. Both temperature and pressure decreased at the nozzle's converging portion. A sudden shift in temperature and pressure was caused by condensation shock, which happens when the flow reaches the throat and proceeds toward the divergent portion of the nozzle. Both temperature and pressure continued to drop as the flow passed through the nozzle after the condensation shock;
- The main findings of this study revealed that the saturated state at the inlet in the converging part of the nozzle had a minimal effect on the Mach number. Nonetheless, significant alterations were seen in the diverging region of the nozzle and the location of the condensation shock. In particular, an increase in the inlet saturation pressure resulted in a rise in the Mach number within the divergent part of the nozzle;
- An increase in the saturation pressure at the nozzle inlet correlated with a rise in the droplet radius. The droplet radius at the nozzle outlet was recorded as 138.6 nm, 240.4 nm, 264.6 nm, and 287.0 nm for the saturation pressures of 25 kPa, 50 kPa, 75 kPa, and 100 kPa, respectively;
- At 25 kPa, 50 kPa, 75 kPa, and 100 kPa saturation pressures, the nozzle outlet's fluid mass fraction was around 0.0606, 0.062, 0.065, and 0.066, respectively. A 9.65% increase in the liquid mass fraction resulted from raising the intake saturation pressure from 25 kPa to 100 kPa.

In future studies, it is suggested to investigate the effect of liquid droplet formation and growth in high-pressure flow conditions and in the saturated state.

Author Contributions: Conceptualization, S.J.K.; methodology, S.J.K.; software, M.A.; validation, S.J.K. and M.A.; formal analysis, S.J.K. and M.A.; resources, S.J.K. and M.A.; data curation, S.J.K.; writing—original draft preparation, S.J.K.; writing—review and editing, M.A.; visualization, S.J.K.; supervision, M.A.; project administration, S.J.K. and M.A.; funding acquisition, S.J.K. and M.A. All authors have read and agreed to the published version of the manuscript.

Funding: This research received no external funding.

Data Availability Statement: The data presented in this study are available on request from the corresponding author.

Conflicts of Interest: The authors declare no conflicts of interest.

References

1. Xia, R.; Li, D.; Faghih Aliabadi, M.A. A comprehensive investigation and optimization of superheat degree on performance of supersonic nozzle by considering non-equilibrium condensation and entropy generation analysis. *Phys. Fluids* **2024**, *36*, 096116. [CrossRef]
2. Mottahedi, H.R.; Aliabadi, M.A.; Gharehbaei, H.; Iraj, L.; Bouzari, S.; Akrami, M. Effects of motive flow temperature on holding steam ejector performance under condenser temperature change by considering entropy generation and non-equilibrium condensation. *Appl. Therm. Eng.* **2024**, *257*, 124268. [CrossRef]
3. Dolatabadi, A.M.; Mottahedi, H.R.; Aliabadi, M.A.; Pour, M.S.; Wen, C.; Akrami, M. Evaluating and optimizing of steam ejector performance considering heterogeneous condensation using machine learning framework. *Energy* **2024**, *305*, 132240. [CrossRef]
4. Wen, C.; Ding, H.; Yang, Y. Optimisation study of a supersonic separator considering nonequilibrium condensation behaviour. *Energy Convers. Manag.* **2020**, *222*, 113210. [CrossRef]
5. Chen, J.; Li, A.; Huang, Z.; Jiang, W.; Xi, G. Non-equilibrium condensation in flue gas and migration trajectory of CO_2 droplets in a supersonic separator. *Energy* **2023**, *276*, 127589. [CrossRef]
6. Chen, J.; Huang, Z.; Jiang, W. Non-equilibrium condensation of carbon dioxide in flue gas with the coexistence of swirl flows and supersonic flows. *Int. Commun. Heat Mass Transf.* **2022**, *138*, 106369. [CrossRef]
7. Zhang, G.; Li, Y.; Jin, Z.; Dykas, S.; Cai, X. A novel carbon dioxide capture technology (CCT) based on non-equilibrium condensation characteristics: Numerical modelling, nozzle design and structure optimization. *Energy* **2024**, *286*, 129603. [CrossRef]
8. Sun, W.; Pen, J.; Niu, L.; Jiang, Z.; Hu, W.; Pan, L.M. Sensitivity analysis of nucleation and droplet growth models in the prediction of natural gas non-equilibrium condensation in Laval nozzle. *Appl. Therm. Eng.* **2024**, *236*, 121562. [CrossRef]
9. Shooshtari, S.R.; Shahsavand, A. Maximization of energy recovery inside supersonic separator in the presence of condensation and normal shock wave. *Energy* **2017**, *120*, 153–163. [CrossRef]
10. Faghih Aliabadi, M.A.; Mahpeykar, M.R. Comparison between polydispersed and monodispersed models on condensing water-vapor flow in a supersonic convergent-divergent nozzle. *Modares Mech. Eng.* **2017**, *17*, 19–30. Available online: https://mme.modares.ac.ir/files/mme/user_files_749497/mahpeykar-A-15-12075-1-ec8667f.pdf (accessed on 10 December 2024).
11. Dolatabadi, A.M.; Masoumi, S.; Lakzian, E. Optimization variables of the injection of hot-steam into the non-equilibrium condensing flow using TOPSIS method. *Int. Commun. Heat Mass Transf.* **2021**, *129*, 105674. [CrossRef]
12. Starzmann, J.; Hughes, F.R.; White, A.J.; Grübel, M.; Vogt, D.M. Numerical investigation of boundary layers in wet steam nozzles. *Turbo Expo Power Land Sea Air* **2016**, *49866*, V008T26A037. [CrossRef]
13. Dykas, S.; Majkut, M.; Smołka, K.; Strozik, M. An attempt to make a reliable assessment of the wet steam flow field in the de Laval nozzle. *Heat Mass Transf.* **2018**, *54*, 2675–2681. [CrossRef]
14. Dykas, S.; Majkut, M.; Smołka, K.; Strozik, M. Experimental research on wet steam flow with shock wave. *Exp. Heat Transf.* **2015**, *28*, 417–429. [CrossRef]
15. Han, X.; Guan, J.; Zhu, Q.; Han, Z. Application of quadratic regression orthogonal design to optimization surface heating for control wet steam condensation flow in nozzle. *Case Stud. Therm. Eng.* **2022**, *34*, 101987. [CrossRef]
16. Halama, J.; Hric, V. Numerical solution of steam flow in a nozzle using different non-equilibrium condensation models. *Appl. Math. Comput.* **2016**, *272*, 657–669. [CrossRef]
17. Sun, W.; Chen, S.; Hou, Y.; Bu, S.; Ma, Z.; Zhang, L. Numerical studies of nitrogen spontaneous condensation flow in laval nozzles using varying droplet growth models. *Int. J. Multiph. Flow* **2019**, *121*, 103118. [CrossRef]
18. Lin, L.; Cheng, W.; Luo, X.; Qin, F. On nitrogen condensation in hypersonic nozzle flows: Numerical method and parametric study. *Shock. Waves* **2014**, *24*, 179–189. [CrossRef]
19. Aliabadi, M.A.; Bahiraei, M. Effect of water nano-droplet injection on steam ejector performance based on non-equilibrium spontaneous condensation: A droplet number study. *Appl. Therm. Eng.* **2021**, *184*, 116236. [CrossRef]
20. Aliabadi, M.A.; Jahangiri, A.; Khazaee, I.; Lakzian, E. Investigating the effect of water nano-droplets injection into the convergent-divergent nozzle inlet on the wet steam flow using entropy generation analysis. *Int. J. Therm. Sci.* **2020**, *149*, 106181. [CrossRef]
21. Aliabadi, M.A.; Zhang, G.; Dykas, S.; Li, H. Control of two-phase heat transfer and condensation loss in turbine blade cascade by injection water droplets. *Appl. Therm. Eng.* **2021**, *186*, 116541. [CrossRef]
22. Zhang, G.; Wang, X.; Chen, J.; Tang, S.; Smołka, K.; Majkut, M.; Jin, Z.; Dykas, S. Supersonic nozzle performance prediction considering the homogeneous-heterogeneous coupling spontaneous non-equilibrium condensation. *Energy* **2023**, *284*, 129274. [CrossRef]
23. Zhang, G.; Wang, X.; Dykas, S.; Aliabadi, M.A. Reduction entropy generation and condensation by NaCl particle injection in wet steam supersonic nozzle. *Int. J. Therm. Sci.* **2022**, *171*, 107207. [CrossRef]
24. Zhang, G.; Wang, X.; Wiśniewski, P.; Chen, J.; Qin, X.; Dykas, S. Effect of NaCl presence caused by salting out on the heterogeneous-homogeneous coupling non-equilibrium condensation flow in a steam turbine cascade. *Energy* **2023**, *263*, 126074. [CrossRef]

25. Hosseini, R.; Lakzian, E. Optimization volumetric heating in condensing steam flow by a novel method. *J. Therm. Anal. Calorim.* **2020**, *140*, 2421–2433. [CrossRef]
26. Hoseinzade, D.; Lakzian, E.; Hashemian, A. A blackbox optimization of volumetric heating rate for reducing the wetness of the steam flow through turbine blades. *Energy* **2021**, *220*, 119751. [CrossRef]
27. Vatanmakan, M.; Lakzian, E.; Mahpeykar, M.R. Investigating the entropy generation in condensing steam flow in turbine blades with volumetric heating. *Energy* **2018**, *147*, 701–714. [CrossRef]
28. Salimi, J.; Teymourtash, A.R.; Aghdasi, M.R.; Lakzian, E. Optimization of the surface heating for a stationary cascade turbine blade in wet steam flow. *Therm. Sci. Eng. Prog.* **2023**, *39*, 101751. [CrossRef]
29. Han, X.; Yuan, Y.; Zhao, Z.; Wang, Y.; Zeng, W.; Han, Z. Numerical investigation of the wet steam condensation flow characteristics in stator cascade with blade surface heating. *Eng. Appl. Comput. Fluid Mech.* **2020**, *14*, 1251–1262. [CrossRef]
30. Hosseinizadeh, S.E.; Ghamati, E.; Jahangiri, A.; Majidi, S.; Khazaee, I.; Aliabadi, M.A. Reduction of water droplets effects in steam turbine blade using Multi-objective optimization of hot steam injection. *Int. J. Therm. Sci.* **2023**, *187*, 108155. [CrossRef]
31. Aliabadi, M.A.; Lakzian, E.; Khazaei, I.; Jahangiri, A. A comprehensive investigation of finding the best location for hot steam injection into the wet steam turbine blade cascade. *Energy* **2020**, *190*, 116397. [CrossRef]
32. Mirhoseini, M.S.; Boroomand, M. Control of wetness fraction and liquid droplet size in wet steam two phase flows with hot steam injection. *Meccanica* **2018**, *53*, 193–207. [CrossRef]
33. Dolatabadi, A.M.; Lakzian, E.; Heydari, M.; Khan, A. A modified model of the suction technique of wetness reducing in wet steam flow considering power-saving. *Energy* **2022**, *238*, 121685. [CrossRef]
34. Taheri, M.R.; Soleymani, A.; Toloei, A.; Vali, A.R. Performance Evaluation of the High-altitude Launch Technique to Orbit Using Atmospheric Properties. *Int. J. Eng.* **2013**, *26*, 333–340. [CrossRef]
35. Hosseini, S.A.; Nakisa, M.; Lakzian, E. Reducing the condensing flow effects on the steam turbine blades through modified design geometry. *Phys. Fluids* **2023**, *35*, 0166144. [CrossRef]
36. Talebi Somesaraee, M.; Amiri Rad, E.; Mahpeykar, M.R. Analytical investigation of simultaneous effects of convergent section heating of Laval nozzle, steam inlet condition, and nozzle geometry on condensation shock. *J. Therm. Anal. Calorim.* **2018**, *133*, 1023–1039. [CrossRef]
37. Ma, Q.F.; Hu, D.P.; Jiang, J.Z.; Qiu, Z.H. A turbulent Eulerian multi-fluid model for homogeneous nucleation of water vapour in transonic flow. *Int. J. Comput. Fluid Dyn.* **2009**, *23*, 221–231. [CrossRef]
38. Zhang, G.; Dykas, S.; Majkut, M.; Smołka, K.; Cai, X. Experimental and numerical research on the effect of the inlet steam superheat degree on the spontaneous condensation in the IWSEP nozzle. *Int. J. Heat Mass Transf.* **2021**, *165*, 120654. [CrossRef]
39. Mahpeykar, M.R.; Teymourtash, A.R.; Amiri Rad, E. Reducing entropy generation by volumetric heat transfer in a supersonic two-phase steam flow in a Laval nozzle. *Int. J. Exergy* **2011**, *9*, 21–39. [CrossRef]
40. Mahpeykar, M.R.; Teymourtash, A.R.; Amiri Rad, E. Theoretical investigation of effects of local cooling of a nozzle divergent section for controlling condensation shock in a supersonic two-phase flow of steam. *Meccanica* **2013**, *48*, 815–827. [CrossRef]
41. Hosseini, S.A.; Lakzian, E.; Nakisa, M. Multi-objective optimization of supercooled vapor suction for decreasing the nano-water droplets in the steam turbine blade. *Int. Commun. Heat Mass Transf.* **2023**, *142*, 106613. [CrossRef]
42. Sharifi, N. Numerical study of non-equilibrium condensing supersonic steam flow in a jet-pump based on supersaturation theory. *Int. J. Mech. Sci.* **2020**, *165*, 105221. [CrossRef]
43. Mehrpooya, M.; Ghafoorian, F.; Farajyar, S. 3D-modeling of a coaxial borehole heat exchanger in Sahand Field, Northwest Iran considering the porous medium and presence of nanofluids. *Iran. J. Chem. Chem. Eng.* **2023**, *42*, 3898–3916. Available online: https://www.ijcce.ac.ir/article_704598_a72776459aec7106f3c9abed5f1a58b2.pdf (accessed on 10 December 2024).
44. Farajyar, S.; Ghafoorian, F.; Mehrpooya, M.; Asadbeigi, M. CFD investigation and optimization on the aerodynamic performance of a Savonius vertical axis wind turbine and its installation in a hybrid power supply system: A case study in Iran. *Sustainability* **2023**, *15*, 5318. [CrossRef]
45. Fu, M.; Ding, Y. Investigating the effects of outlet pressure from steam turbine blade on wetness and entropy generation with consideration of non-equilibrium condensation. *Comput. Therm. Sci. Int. J.* **2023**, *15*, 61–73. [CrossRef]
46. Dolatabadi, A.M.; Pour, M.S.; Ajarostaghi, S.S.; Poncet, S.; Hulme-Smith, C. Last stage stator blade profile improvement for a steam turbine under a non-equilibrium condensation condition: A CFD and cost-saving approach. *Alex. Eng. J.* **2023**, *73*, 27–46. [CrossRef]
47. Lai, S.; Wang, W. A comprehensive investigation of two-phase flow in off-design operating condition of ejector performance by using entropy generation analysis. *Proc. Indian Natl. Sci. Acad.* **2024**, 1–3. [CrossRef]
48. Hui, X.; Ma, Y.; Deng, X. Numerical simulation on effects of augmentation in temperature of inlet steam on wet steam flow in supersonic nozzle: Energy and exergy analysis. *Multiscale Multidiscip. Model. Exp. Des.* **2023**, *6*, 723–732. [CrossRef]
49. Xu, Y.; Zhang, X.; Bai, Y.; Li, X. Numerical investigation of liquid mass fraction and condensation shock of wet-steam flow through convergence-divergence nozzle using strategic water droplets injection. *Chem. Prod. Process. Model.* **2023**, *19*, 315–327. [CrossRef]
50. Wu, Z.; Gang, J. Numerical investigation of exit pressure on flow structure in steam ejector by considering condensation and evaporation process. *Proc. Indian Natl. Sci. Acad.* **2024**, *90*, 113–123. [CrossRef]
51. Zhao, S.; Li, X.; Jia, Z. Relation between the divergent section's angle and two-phase heat in the condensation flow of wet steam in a supersonic nozzle. *Multiscale Multidiscip. Model. Exp. Des.* **2023**, *7*, 777–785. [CrossRef]

52. Dolatabadi, A.M.; Aliabadi, M.A. Evaluating sustainability power plant efficiency: Unveiling the impact of power plant load ratio on holding steam ejector performance. *Energy* **2024**, *305*, 132315. [CrossRef]
53. Aliabadi, M.A.; Lakzian, E.; Jahangiri, A.; Khazaei, I. Numerical investigation of effects polydispersed droplets on the erosion rate and condensation loss in the wet steam flow in the turbine blade cascade. *Appl. Therm. Eng.* **2020**, *164*, 114478. [CrossRef]
54. Jahangiri, A.; Aliabadi, M.A.; Pourranjbar, D.; Mottahedi, H.R.; Gharebaei, H.; Ghamati, E. A comprehensive investigation of non-condensable gas and condenser temperature effects on power plant ejector performance by considering condensation flow regime. *Therm. Sci. Eng. Prog.* **2023**, *45*, 102128. [CrossRef]
55. Cong, H.; Zhang, J. Numerical investigation of the effects of dry gas model and wet steam model in solar-driven refrigeration ejector system. *Chem. Prod. Process Model.* **2024**, *19*, 69–80. [CrossRef]
56. Wang, H.Z. Energy and exergy analysis of primary steam superheating effects on the steam ejector applied in the solar renewable refrigeration cycle in the presence of spontaneous nucleation. *Chem. Prod. Process. Model.* **2024**, *19*, 51–68. [CrossRef]
57. Kermani, M.J.; Gerber, A.G. A general formula for the evaluation of thermodynamic and aerodynamic losses in nucleating steam flow. *Int. J. Heat Mass Transf.* **2003**, *46*, 3265–3278. [CrossRef]
58. Ma, C.; Wang, S.; Yu, J. Numerical Study on the Influence of Separation Time Sequence on the Initial Thermal Separation. *Energies* **2024**, *17*, 1598. [CrossRef]
59. Volov, V.; Elisov, N.; Lyaskin, A. Numerical Investigation of the Secondary Swirling in Supersonic Flows of Various Nature Gases. *Energies* **2021**, *14*, 8122. [CrossRef]
60. Murugesan, P.; Srikrishnan, A.R.; Mohammad, A.; Velamati, R.K. Numerical Study of Wall Heat Transfer Effects on Flow Separation in a Supersonic Overexpanded Nozzle. *Energies* **2023**, *16*, 1762. [CrossRef]
61. Ghafoorian, F.; Mirmotahari, S.R.; Eydizadeh, M.; Mehrpooya, M. A systematic investigation on the hybrid Darrieus-Savonius vertical axis wind turbine aerodynamic performance and self-starting capability improvement by installing a curtain. *Next Energy* **2024**, *6*, 100203. [CrossRef]

Disclaimer/Publisher's Note: The statements, opinions and data contained in all publications are solely those of the individual author(s) and contributor(s) and not of MDPI and/or the editor(s). MDPI and/or the editor(s) disclaim responsibility for any injury to people or property resulting from any ideas, methods, instructions or products referred to in the content.